Magnetic properties of the covalent chain antiferromagnet $RbFeSe_2$

Z. Seidov,[1,2] H.-A. Krug von Nidda,[1,*] V. Tsurkan,[1,3] I. G. Filippova,[3] A. Günther,[1] T. P. Gavrilova,[4] F. G. Vagizov,[5] A. G. Kiiamov,[5] L. R. Tagirov,[4,5] and A. Loidl[1]

[1]*Experimental Physics V, Center for Electronic Correlations and Magnetism, University of Augsburg, 86135 Augsburg, Germany*

[2]*Institute of Physics, Azerbaijan National Academy of Sciences, AZ-1143 Baku, Azerbaijan*

[3]*Institute of Applied Physics, Academy of Sciences of Moldova, MD-20208 Chisinau, Moldova*

[4]*E. K. Zavoisky Physical-Technical Institute, Russian Academy of Sciences, 420029 Kazan, Russia*

[5]*Institute of Physics, Kazan Federal University, 420008 Kazan, Russia*

(Received 30 May 2016; revised manuscript received 1 September 2016; published 13 October 2016)

Single crystals of the ternary iron selenide $RbFeSe_2$ have been investigated by means of x-ray diffraction, magnetic susceptibility, magnetization, and specific-heat measurements as well as by Mössbauer spectroscopy. Built up from linear chains of edge-sharing $FeSe_4$ tetrahedra, $RbFeSe_2$ represents a quasi-one-dimensional antiferromagnet. Below $T_N = 248$ K three-dimensional antiferromagnetic collinear magnetic order sets in, with the magnetic moments oriented perpendicularly to the chain direction. The hyperfine fields determined from our Mössbauer studies reveal strongly reduced magnetic moments. The high-temperature susceptibility data of $RbFeSe_2$ suggest a one-dimensional metallic character along the chains.

DOI: 10.1103/PhysRevB.94.134414

I. INTRODUCTION

The recent discovery of iron-based superconductors [1–4] has stimulated high interest and enormous scientific activities in the field of iron-pnictide and -chalcogenide materials. Notably, all iron-based superconductors exhibit some structural similarity. From the initially discovered $LaFeAsO_{1-x}F_x$ to recently reported $K_xFe_{2-y}Se_2$ and $(Tl,K)Fe_{2-x}Se_2$, two-dimensional (2D) layers of FePn or FeCh (Pn = pnictogens, Ch = chalcogens) tetrahedra are the common structural units [5–9]. The mechanism of superconductivity and its relation to the crystal structure in these systems is still under debate. In particular, the question concerning localization or delocalization of the magnetic moments of iron deserves intense consideration. Therefore, in order to achieve deeper insight into the nature of superconductivity, the study of materials containing similar building blocks related to these systems is of significant interest. In this respect, it is important to note that currently pressure-induced superconductivity has been discovered even in the 1D spin-ladder compound $BaFe_2S_3$ consisting of FeS_4 tetrahedra as well [10].

Systematic structural investigations of ternary metal chalcogenides $A_xFe_yX_z$ (A = alkali metal, Tl; X = S, Se) have revealed a variety of distinct compositions with tetrahedral $[FeX_4]$ structural units, i.e., A_5FeX_4, AFe_2X_2, AFe_2X_3, A_3FeX_3, $AFeX_2$, and $A_3Fe_2S_4$ [11–19]. The chalcogenide crystals Na_5FeS_4, A_3FeX_3 (A = Na, Cs; X = S, Se), and $AFeX_2$ (A = K, Cs; X = S, Se) consist of discrete tetrahedral $[FeS_4]^{5-}$ complexes [14], edge-linked double tetrahedral $[Fe_2X_6]^{6-}$ complexes [15,20,21], or one-dimensional $^1_\infty[FeX_{4/2}]^-$ chains [15,22,23], respectively. Magnetic susceptibility measurements revealed a systematic reduction of the local iron-spin moment $S = 5/2$ of discrete tetrahedra down to $S = 3/2$ in double-tetrahedral complex and towards $S = 1/2$ in chain compounds [14,15,20–24].

In this work we concentrate on $RbFeSe_2$ chalcogenide, which belongs to the group of one-dimensional compounds $AFeX_2$ consisting of linear chains of edge-sharing $[FeX_4]$ tetrahedra along the c direction separated by Rb atoms (see Fig. 1). Concerning the question about the relation of superconductivity and magnetism, these linear chain compounds serve as useful model systems, because the small Fe-Fe intrachain separation gives rise to strong covalence effects and is expected to promote spin reduction and charge-carrier delocalization on the verge to 1D metallic behavior.

The crystallographic and magnetic data for $AFeX_2$ (A = K, Rb, Cs, Tl; X = S, Se) are collected in Table I. In their magnetic properties, the iron compounds can be divided into three groups as follows (see references in Tiwary and Vasudevan [24], Seidov *et al.* [25], Asgerov *et al.* [26], Nishi and Ito [27,28], Welz *et al.*[29–32], and Bronger and Müller [15,22]):

(1) monoclinic $TlFeS_2$, $TlFeSe_2$, $KFeSe_2$, and $RbFeSe_2$ with the magnetic moments ordered perpendicular to the chains;

(2) orthorhombic $CsFeS_2$ with no magnetic order down to the structural transition at $T_{struc} = 70$ K (below T_{struc} with orientation of the magnetic moments approximately along the chain direction); and

(3) monoclinic $KFeS_2$, $RbFeS_2$ with the ordered moments slightly tilted from the chain axis.

All these compounds involve formally trivalent iron with a half-filled $3d$ electronic shell. The ordered magnetic moment, far below the ionic high-spin value of $5\mu_B$, indicates a considerable $3d$ delocalization, which has been attributed to intimate Fe contact resulting from the in-chain Fe distance, not much exceeding the Fe-Fe distance (2.48 Å) of metallic iron. Hence, a certain degree of itinerancy along the chains and concomitant one-dimensional metallic behavior can be expected.

In this article we present x-ray diffraction, magnetization, specific-heat, and Mössbauer experiments on single-crystalline $RbFeSe_2$. The comparison of our results with those of related 1D and 2D iron chalcogenides and pnictides is

*hans-albrecht.krug@physik.uni-augsburg.de

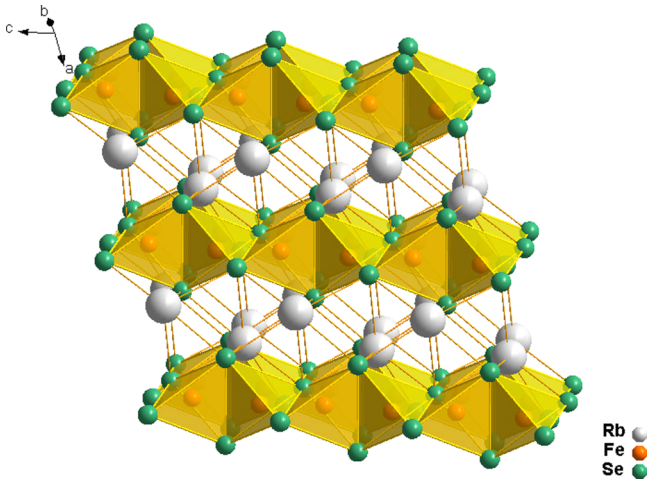

FIG. 1. Crystal structure of $RbFeSe_2$. The $FeSe_4$ tetrahedra, with Fe drawn as orange sphere in the center and Se as green sphere at the corners, are highlighted in transparent yellow color. White large spheres denote Rb.

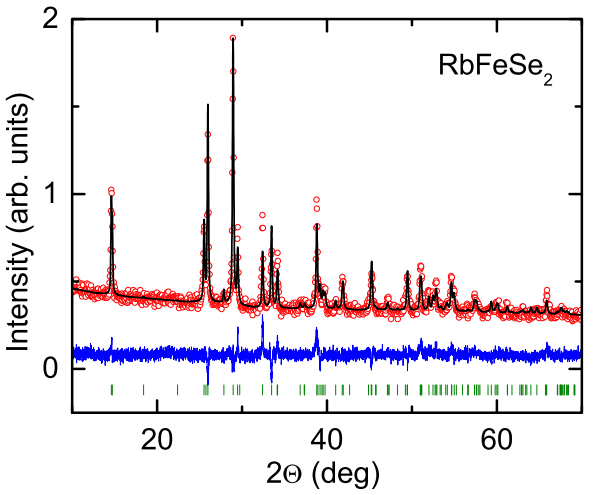

FIG. 2. Powder diffraction pattern of $RbFeSe_2$. The empty circles represent the measured intensities. The black solid line shows the refined pattern. The Bragg-peak positions are indicated by vertical (green) bars. The difference pattern $I_{obs} - I_{cal}$ is indicated by the solid (blue) line.

important for revealing the intrinsic electronic properties of this class of materials.

II. RESULTS AND DISCUSSION

A. Preparation, x-ray diffraction, and crystal structure

Single crystals of $RbFeSe_2$ were grown by the Bridgman method. The needlelike shape of the crystals indicates the one-dimensionality of the structure. The constituent fibers are mechanically strong, but they bend and can be separated easily. Fresh surfaces have a silver-metallic appearance. The elemental composition was determined by wavelength dispersive x-ray electron-probe microanalysis (WDS EPMA, Cameca SX50) to be 24.74 (89) at% for Rb, 24.74(57) at% for Fe, and 50.52(98) at% for Se, respectively, resulting in the composition $Rb_{0.98}Fe_{0.98}Se_{2.00}$ indicating minor deviation of the sample composition from stoichiometric $RbFeSe_2$.

TABLE I. Crystallographic and magnetic data for $AFeX_2$ (A = K, Rb, Cs, Tl; X = S, Se).

Sample	Space group	d (Å) (Fe-Fe)	T_N (K)	Moment orientation	μ_{ord} (μ_B)	Ref.
$KFeS_2$	$C2/c$	2.70 uniform	250	13° from chain	2.43	[15,22,24] [27,29]
$RbFeS_2$	$C2/c$	2.71 uniform	188	∥ chain slightly tilted	1.83	[15,22]
$CsFeS_2$	$Immm$	2.61 dimerized	–	below T_{struc} close to chain	1.88	[24,28,32]
$TlFeS_2$	$C2/m$	2.65 dimerized	196	⊥ chain	1.85	[17,25] [30,31]
$KFeSe_2$	$C2/c$	2.81 uniform	310	⊥ chain	3	[15,22]
$RbFeSe_2$	$C2/c$	2.83 uniform	250	⊥ chain	2.66	[15,22]
$TlFeSe_2$	$C2/m$	2.74 uniform	290	⊥ chain	2.1	[25,26]

The structural details of the crystals were investigated by conventional x-ray diffraction on powdered single crystals at room temperature using a STOE STADI P diffractometer with CuK_α radiation. A typical diffraction profile is shown in Fig. 2. The data were analyzed by standard Rietveld refinement using the program FULLPROF [33]. We could not detect any impurity phases above the background. The structural analysis confirmed the $C2/c$ monoclinic structure for $RbFeSe_2$ with lattice parameters $a = 7.476(5)$ Å, $b = 12.100(8)$ Å, $c = 5.666(3)$ Å, and $\beta = 112.405(3)°$. Except for the lattice constant b, our data are very close to those from Ref. [22] obtained by single-crystal diffraction. We notice that the refinement cannot fully describe the observed peak intensities which can result from a combined effect of stacking faults and strain of the sample when crushed into powder. Table II shows the interatomic distances and angles obtained from the refinement of the crystal structure. The data show that there exist two short [2.325(6) Å] and two long [2.434(7) Å] Fe-Se distances and four different Se-Fe-Se angles indicating strong distortion of the $FeSe_4$ tetrahedra. The shorter Fe-Se distance is remarkably lower than the sum of the covalent radii ($r_{Fe} + r_{Se} = 2.42$ Å) [34,35] while the longer one is close to it. The Fe-Fe distance of 2.850(1) Å exceeds the Fe-Fe distance in metallic iron by about 14%. The deviation of the crystallographic data obtained on our crystals from those reported earlier in Ref. [22] most probably results from the difference in the sample composition due to difference in the preparation methods.

B. Magnetic susceptibility

A commercial superconducting quantum interference device, SQUID MPMS5 magnetometer from Quantum Design, was used to measure magnetic susceptibility $\chi = M/H$ and magnetization M of single crystalline samples within a

TABLE II. $RbFeSe_2$ interatomic distances and angles. Because of the distortion of the $FeSe_4$, the distances between the lattice constituents (and the Se-Fe-Se angles in the tetrahedra) differ. All of them except duplicated [indicated by (×2)] are given in the table.

Bond	Distance (Å)	Angle	(°)
Fe-Se(×2)	2.434(7)	Se-Fe-Se(×2)	106.5(3)
Fe-Se(×2)	2.325(6)	Se-Fe-Se	120.3(4)
Se-Se(×2)	3.812(5)	Se-Fe-Se(×2)	108.5(3)
Se-Se(×2)	3.862(7)	Se-Fe-Se	105.7(3)
Se-Se	3.880(8)		
Se-Se	4.034(6)		
Fe-Fe	2.850(1)		
Rb-Se(×2)	3.616(6)		
Rb-Se(×2)	3.647(5)		
Rb-Se(×2)	3.581(6)		
Rb-Se(×2)	3.482(5)		
Rb-Rb	4.407(7)		
Rb-Rb	4.593(6)		
Rb-Fe	4.039(3)		
Rb-Fe	4.162(4)		
Rb-Fe	4.520(9)		

temperature range $1.8 \leqslant T \leqslant 720$ K and in magnetic fields H up to 50 kOe. Figure 3 shows the magnetic susceptibility of $RbFeSe_2$ as a function of temperature for the magnetic field applied parallel and perpendicular to the chain direction. Note that, due to geometrical restrictions, the sample could not be measured for the magnetic field applied perpendicular to the chain in the oven covering temperatures above 400 K.

Below the Néel temperature $T_N = 248$ K, as in classical antiferromagnets, the susceptibility splits into parallel and perpendicular components with the magnetic moment aligned approximately along the crystallographic b axis ($H \perp c$). Also the linear increase of the magnetization with increasing field below and above T_N, which is shown in the inset of Fig. 3 for the magnetic field applied along the chain direction ($H \| c$), is characteristic for antiferromagnets. The data are

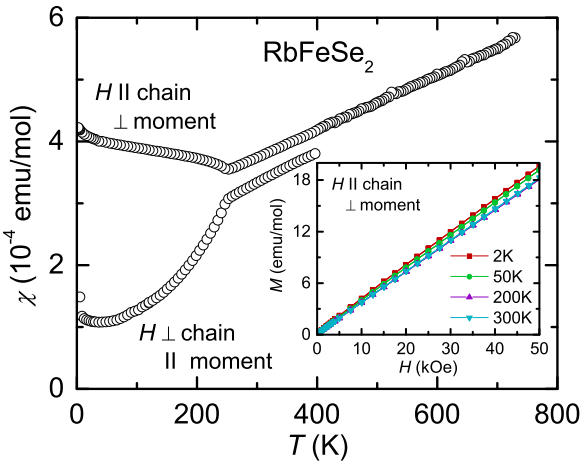

FIG. 3. Temperature dependence of the magnetic susceptibility in $RbFeSe_2$ single crystals parallel and perpendicular to the chain direction ($H = 10$ kOe). Inset: Field dependence of the magnetization along the chain direction in $RbFeSe_2$ at different temperatures.

in good agreement with neutron-diffraction and Mössbauer measurements published by W. Bronger *et al.* [22] and H. Nissen and K. Nagorny [36]. To lowest temperatures the susceptibility χ approaches a value of 4.2×10^{-4} emu/mol for the field applied perpendicular to the ordered moment ($H \| c$) and 1.2×10^{-4} emu/mol for the field applied parallel to the ordered moment ($H \| b$). For temperatures $T > T_N$ the susceptibility increases linearly with increasing temperature with isotropic slope but anisotropic offset. This linear increase of the susceptibility up to 720 K is rather unusual for 1D antiferromagnetic (AFM) Heisenberg chains of localized spins, which typically exhibit a susceptibility maximum at a temperature comparable to the intrachain exchange. Such susceptibility maxima have been observed, e.g., in the related alkaline K and Cs iron sulfides at $T_{max} = 565$ K for $KFeS_2$ and $T_{max} = 800$ K for $CsFeS_2$, where the temperature dependence of the susceptibility could be approximated using the model of an AFM spin $S = 1/2$ chain [24]. On the other hand, for $TlFeS_2$ and $TlFeSe_2$, the susceptibility increases linearly above T_N without any tendency to saturation [25] like for $RbFeSe_2$ considered here. It seems that in this compound, via the strong and direct Fe-Fe exchange, a fraction of the d electrons is close to delocalization.

This is reminiscent of the organic tetramethyl-tetrathia fulvalen $(TMTTF)_2X$ and tetramethyl-tetraselenium fulvalen $(TMTSF)_2X$ linear-chain spin $S = 1/2$ compounds with, e.g., $X = PF_6$, AsF_6, and Br [37], where the degree of delocalization of charge carriers is very sensitive to the chemical composition. While the sulfur compound $(TMTTF)_2PF_6$ shows charge localization and a maximum in the susceptibility close to 300 K, the corresponding selenium compound $(TMTSF)_2PF_6$ is a one-dimensional metal, and its susceptibility increases approximately linearly from the spin-density wave (SDW) transition at $T_{SDW} = 12$ K up to 500 K, which was the highest accessible temperature in that experiment. Thus, one could expect 1D conductivity in $RbFeSe_2$. However, like in $TlFeS_2$ and $TlFeSe_2$ [25], we were not able to establish metallic conductivity in $RbFeSe_2$ by resistivity measurements. As mentioned in Ref. [25], the single crystals consist of thin fibers which are difficult to treat, because they easily break into pieces. To prove 1D conductivity, it would be desirable to probe the current within the fibers. However, defects and mechanical breaks in the chains are inevitable and, therefore, they obviously terminate the conductivity, resulting in an increasing resistivity with decreasing temperature. This idea is in agreement with Nashioka *et al.* [38,39], who predicted the alkaline compound $KFeS_2$ to be metallic on a microscopic scale despite macroscopic semiconducting behavior. For this reason, resistance measurements do not seem to be reliable, and it is necessary to look carefully for metallic behavior in other properties. The investigations of the electronic structure of $TlFeX_2$ (X = S, Se) by photoemission suggest an itinerant nature of the Fe electrons in these compounds [40]. In particular, the Fe $2p$ core level indicates an itinerant behavior [41,42].

Note that a linear increase of the magnetic susceptibility with increasing temperature was also observed in some two-dimensional metallic layered iron pnictides above the SDW phase transition or above the superconducting phase, like in $BaFe_2As_2$ (Fe-Fe distances 2.81 Å) [43,44] $Ca(Fe_{1-x}Co_x)_2As_s$, or $LaFeASO_{1-x}F_x$ [45]. It is now well

established that such a linear increase of the magnetic susceptibility with temperature is a general property of Fe pnictides in the paramagnetic regime [3]. Wang *et al.* [43] and Zang *et al.*[46] suggested that the linear temperature behavior is a consequence of strong AFM fluctuations present at ($T > T_{SDW}$). Korshunov *et al.* [47] argued that short-range AFM fluctuations are the source of a linear temperature term in the susceptibility of a two-dimensional Fermi liquid. Kou *et al.*[48] studied a minimal model composed of coupled itinerant electrons and local moments in a mean-field approach. They find that SDW order and superconducting pairing of the itinerant electrons are mainly induced by their coupling to the local moments with momentum match and that the presence of local moments also explains the normal-state linear in temperature magnetic susceptibility above T_{SDW}. Skornyakov *et al.* [49] ascribed the increase of the susceptibility with temperature to thermal excitation of electron states. Application of dynamical mean-field theory (DMFT) to a one-band model with a density of states corresponding to the Fe-d_{xy} spectral function of $BaFe_2As_2$ reveals a peak in the vicinity of the Fermi energy as prerequisite for the linear increase of the magnetic susceptibility.

Moreover, returning to the question of electrical resistivity in $TlFeS_2$, $TlFeSe_2$, and $RbFeSe_2$, it is worthwhile to consider the situation in quasi-2D layered superconducting Fe selenides $Rb_{0.8}Fe_{1.6}Se_2$ ($H \| c$), $Tl_{0.58}Rb_{0.42}Fe_{1.72}Se_2$ and nonsuperconducting (non-SC) Fe selenides ($H \| c$) $Rb_{0.689}Fe_{1.497}Se_2$ (BR19), $Rb_{0.644}Fe_{1.62}Se_2$ (BR22) [50,51], which exhibit linearly increasing magnetic susceptibilities in a wide temperature range due to the fact that their AFM ordering temperatures are significantly above 400 K. Also the related series of compounds (Tl,K)Fe_xSe_2 with ($1.3 \leqslant x \leqslant 1.65$) with a monotonously increasing susceptibility in the paramagnetic regime has to be mentioned [9]. It turned out that the resistivity of the non-SC selenide samples BR22, BR19, and BR17 shows semiconductor-like behavior with decreasing temperature [50]: In the range $300 \geqslant T \geqslant 240$ K, the temperature dependence of the resistivity follows an Arrhenius law with rather low values of activation energies of the order of 100 meV. Such low activation energies are more typical for heavily doped semiconductors or Mott insulators than for intrinsic band insulators. At temperatures below 240 K down to 80 K, the resistivity is not thermally activated anymore but, instead, can be reasonably explained within a Mott variable-range hopping model following $\rho = \rho_0 \exp(T_0/T)^{1/4}$. In the non-SC compounds of the (Tl,K)Fe_xSe_2 series the resistivity follows an Arrhenius law down to approximately $T = 50$ K with comparably small activation energies as in BR22, BR19, and BR17 [9]. Obviously, all these compounds are at the verge of metallic behavior.

C. Specific heat

The specific heat was measured by a relaxation method using a Physical Property Measurement System (PPMS) (Quantum Design) in the temperature range $1.8 \leqslant T \leqslant 300$ K and in magnetic fields up to 90 kOe. The magnetic field was applied perpendicularly to the chain direction of the sample. Figure 4 shows the specific heat $C(T)$ as a function of temperature for $RbFeSe_2$. A small anomaly is observed in the $C(T)$ data at $T_N = 247$ K, below which the $\chi(T)$ data split into parallel and perpendicular branches, evidencing long-range

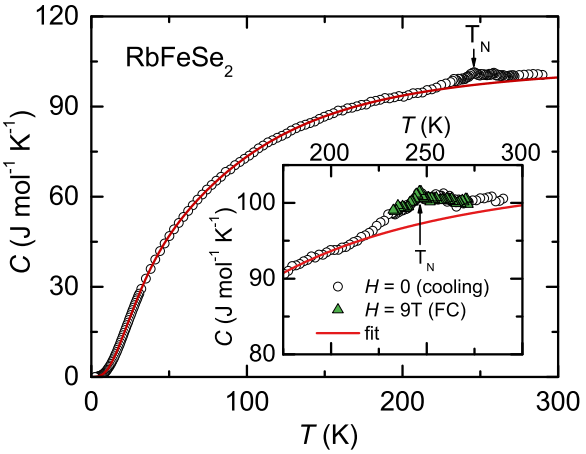

FIG. 4. Temperature dependence of the specific heat $C(T)$ for $RbFeSe_2$. The red solid line indicates the fit to the experimental results by the sum of Debye and Einstein contributions (see details in the text). Inset: Specific heat of $RbFeSe_2$ in the temperature range $175 \leqslant T \leqslant 300$ K measured both on field cooling (FC) and in zero field.

AFM order. In the accessible magnetic-field range the anomaly is field independent.

To estimate the phonon contribution to the specific heat we used the plot C/T vs. T^2 (see Fig. 5), which for low temperatures results in a straight line $C/T = \beta_D T^2$. The slope β_D is determined by the acoustic phonon part of the low-temperature specific heat and allows a direct estimate of the Debye temperature using the formula $\Theta_D = (12\pi^4 R/5\beta_D)^{1/3}$ (where $R = 8.314$ J/molK is the gas constant). From the fit value $\beta_D = 0.225$ mJ/molK, the Debye temperature $\Theta_D = 95$ K was derived. Note that the value of the Debye temperature has to be taken with care, because β_D also contains the contribution of AFM magnons, which cannot be separated from the acoustic phonons.

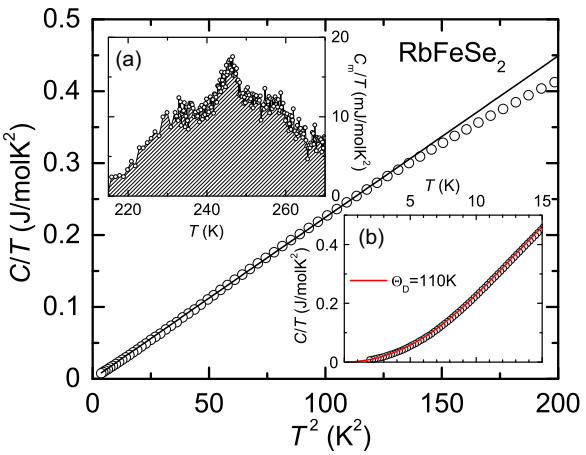

FIG. 5. Specific heat in representation C/T as a function of T^2 for $RbFeSe_2$ at low temperatures (the black solid line is the fitting curve using the formula $C/T = \beta_D T^2$). Insets: (a) High-temperature magnetic specific heat C_M/T versus T in zero external magnetic field for $RbFeSe_2$ after subtracting the calculated lattice contribution; (b) low temperature C/T versus T, the red solid line represents the fit calculated with $\Theta_D = 110$ K.

Based on this estimate, we modelled the specific heat in the full temperature range ($2 \leqslant T \leqslant 300$ K) using two Einstein oscillators and one Debye contribution. Generally, three Einstein oscillators could be expected due to the fact that the formula unit contains four atoms resulting in one Debye and three Einstein oscillators, if one assumes transverse and longitudinal eigenfrequencies to be equal. Moreover, the two Se atoms can be assumed to result in the same eigenfrequency, reducing the number of Einstein oscillators to two. The best fit was achieved with the Debye temperature $\Theta_D = 110$ K ($W_D = 1.59$) and two Einstein temperatures $\Theta_{E_1} = 158$ K ($W_{E_1} = 1.27$) and $\Theta_{E_2} = 520$ K ($W_{E_2} = 1.35$). The fit is displayed as a red solid line in Fig. 4 and focusing on the low-temperature range in Fig. 5(b).

It turns out that the empirical weight (W_D) of the Debye contribution with respect to the Einstein contributions ($W_{E_1} + W_{E_2}$) is larger than expected theoretically, i.e., $W_D : (W_{E_1} + W_{E_2}) > 1 : 3$. In view of the strongly anisotropic crystal structure of $RbFeSe_2$, a consolidation of longitudinal and transverse acoustic phonons into the single Debye oscillator could be a too-crude approximation [52]. Moreover, the total sum of weights ($W_D + W_{E_1} + W_{E_2} = 4.21$) is slightly larger than 4. This can be ascribed to the above-mentioned fact that the contribution of AFM magnons has to be taken into account. Its temperature dependence follows an analogous behavior like the Debye contribution with a characteristic temperature of the order of T_N. As T_N is of the same order of magnitude like Θ_D, the magnon and Debye contributions cannot be separated, thus yielding a higher effective weight of the Debye oscillator and enhanced number of degrees of freedom.

Another useful quantity, which can be extracted from the specific heat, is the entropy loss associated with the AFM ordering of the Fe magnetic moment at the Néel transition. The remaining specific-heat excess in $RbFeSe_2$ is shown in Fig. 5(a). The corresponding entropy value (shaded area below the data) is $\Delta S = 0.52$ J K^{-1}mol^{-1}. This entropy value is much smaller even than $R \ln 2 = 5.76$ J K^{-1}mol^{-1} expected for a low-spin $S = 1/2$ Fe^{3+} spin system. A reduced value of the entropy (3 J K^{-1}mol^{-1}) was also observed in $KFeS_2$ [53]. For $TlFeX_2$ (X = S, Se), specific-heat measurements did not detect an anomaly within the temperature range $4 \leqslant T \leqslant 300$ K [54]. Such an entropy deficit at the magnetic ordering transition is a peculiarity of $TlFeX_2$ (X = S, Se) and AFe_2Se_3 (A = Cs, Ba) [54–56]. This shortfall of the entropy loss at T_N can be ascribed to short-range antiferromagnetic correlations, existing already far above the transition into the long-range AFM order, and to a gradual increase of the magnetic moment below the transition, both characteristic of low-dimensional systems. Hence, the accurate contribution of lattice and electrons to the specific heat needs to be known in a wide temperature range, formally from zero to far above the antiferromagnetic transition temperature T_N, to improve the background subtraction upon calculating the entropy loss at AFM ordering.

D. Mössbauer effect study

Mössbauer spectra were measured at several temperatures in the range $10 \leqslant T \leqslant 300$ K on a conventional constant-acceleration spectrometer (WissEl) equipped with a room-temperature rhodium-matrix cobalt-57 γ-radiation source.

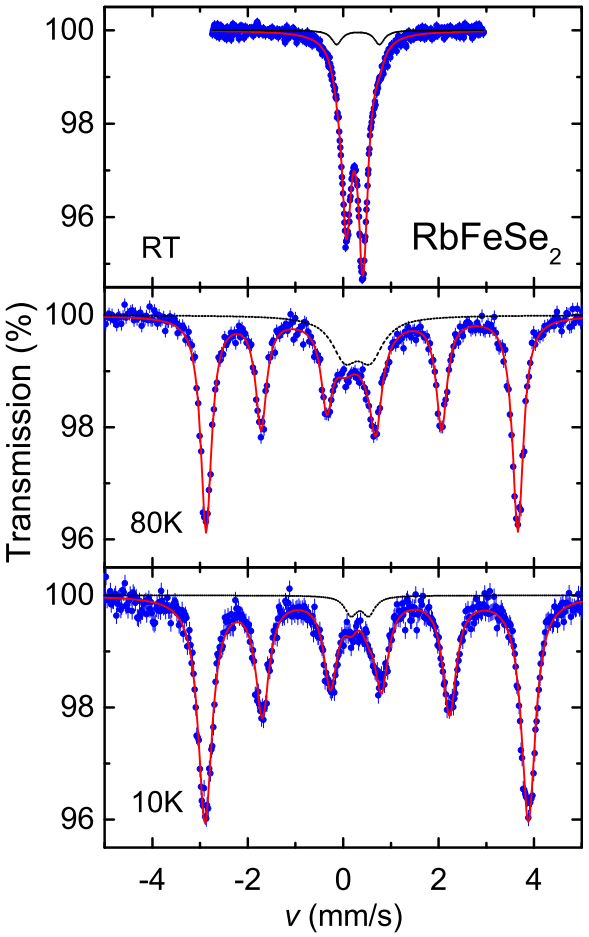

FIG. 6. Selected Mössbauer spectra of $RbFeSe_2$ recorded at room temperature (RT, $T = 300$ K, upper frame), $T = 80$ K (middle frame), and $T = 10$ K (lower frame). Solid red lines represent best fitting of the Mössbauer spectra obtained by least-squares fit with the assumption that the line shapes are Lorentzian. The black dashed line shows the pattern of the paramagnetic doublet coexisting with the magnetic sextet.

The spectrometer was calibrated at room temperature (RT) with an α-iron foil. The absorber was prepared by rubbing the needle-shaped $RbFeSe_2$ crystals on a scotch tape and packing them into a holder closed by thin aluminum foil, all done in an argon-atmosphere dry box. The sample was placed into a cryostat under pure dry argon atmosphere to protect from oxidation and moisture. The temperature of the sample was controlled within ± 0.1 K over the whole temperature range. The observed spectra were least-squares fitted with the assumption that line shapes are Lorentzian to yield the hyperfine parameters, namely isomer shift (IS), quadrupole splitting (QS), and hyperfine field (H_{hf}).

Representative spectra taken at RT and at low temperatures are shown in Fig. 6. The Mössbauer spectrum of $RbFeSe_2$ obtained at RT exhibits an asymmetric doublet typical for paramagnetic iron with quadrupole splitting. The hyperfine parameters are IS = 0.2 mm/s and QS = 0.35 mm/s. Such an asymmetric doublet persists down to $T = 250$ K. The intensity asymmetry of the doublet lines can be explained by preferred orientations of the $RbFeSe_2$ chains all along the surface of the

sample. The rubbing of the needle-shaped crystals on a scotch tape leads to an inherent texture of the sample. Therefore, the relative ratio of the line intensities will differ for π and σ transitions. The smaller intensity of the absorption line located at lower velocity indicates the positive sign of the electric field gradient (EFG). This observation was confirmed by our low-temperature Mössbauer measurements, too.

It is to be noted that the RT spectrum of our sample exhibits a minor quadrupole doublet which contains about 5% of the total spectral area. Its pattern is shown in Fig. 6 by the dashed line. The presence of this doublet can be attributed to those crystal chains which have been deformed during the rubbing, or they were poisoned by oxidation and moisturization. Probably, it is reasonable to guess that the rubbing of the needle-shaped crystals causes strains in the surface of the grains and leads to breaking of the chains. Nevertheless, to assume deterioration is more preferable, because it has been verified that air storage of the sample leads to an increase of this minor doublet intensity.

The Mössbauer isomer shift is found to increase as the temperature is decreased. The total change from $T = 300$ K down to $T = 10$ K is about 0.14 mm/s. This variation can be mainly attributed to the relativistic temperature-dependent contribution to the isomer shift caused by the second-order Doppler shift of the Mössbauer radiation. The RT value of IS of the present measurements is somewhat smaller than that (IS = 0.33 mm/s) reported by Nissen and Nagorny [36].

Since the high-spin ferrous state would generally give larger IS values, the present reduced IS value indicates that the iron in $RbFeSe_2$ is also in a ferric (trivalent) state with relatively strong covalent bonding to selenium ligands. The hint comes from the lower IS values of iron-selenium compounds, compared with those of oxides and fluorides, which is generally attributed to a stronger covalent character in the former. A diminished screening of 4*s* electrons caused by a decrease in 3*d*-electron density at Fe sites can explain the decrease in the isomer shift.

The values for the quadrupole splitting are almost temperature independent except for the jump at $T_N = 248$ K. The quadrupole splitting below the AFM transition was deduced under the assumption that the principal axes of the hyperfine field were parallel to those of the electric field gradient. In this case, the reduction from 0.35 mm/s to 0.22 mm/s, observed at the transition point, may be caused by the change of the ligand contribution to the electric field gradient.

The ^{57}Fe Mössbauer spectroscopy studies were carried out to probe the local magnetic state of the Fe ion in this compound, i.e., to determine the hyperfine field and the magnetic transition temperature. Below the magnetic transition temperature (in our case, the Néel temperature, T_N) a magnetic sextet shows up coexisting with the doublet peak. In Fig. 6 this doublet is shown by a dashed line. Once the temperature is lowered down to $T = 10$ K, the doublet pattern has reduced down to 3% of the total spectral area. The magnetic sextet is due to the well-developed internal hyperfine field indicating the existence of long-range magnetic order. The temperature dependence of the hyperfine field at the ^{57}Fe nucleus is shown in Fig. 7. It can be approximated by the following power law:

$$H_{hf}(T) = H_{0hf}\left(1 - \frac{T}{T_N}\right)^b, \quad (1)$$

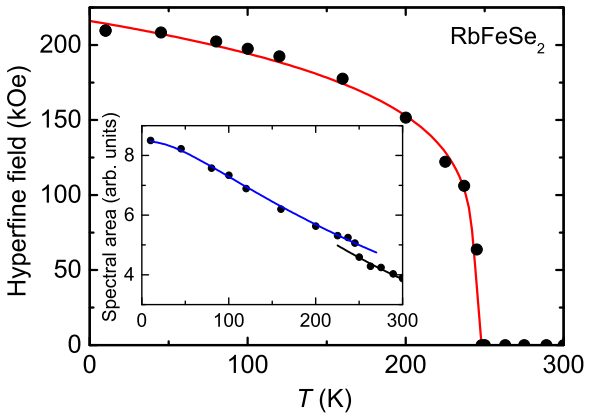

FIG. 7. Temperature dependence of the hyperfine field on the ^{57}Fe nucleus in $RbFeSe_2$. The solid line is obtained by the best least-squares fitting of the data by power law equation (1). Inset: Temperature dependence of the total area below the $RbFeSe_2$ Mössbauer spectrum. The solid lines indicate fits by Eq. (2).

where H_{0hf} is the hyperfine field at the ^{57}Fe nucleus at zero temperature and b denotes the exponent. The experimental data on the temperature dependence of the ^{57}Fe hyperfine field were least-squares fitted by Eq. (1) and allowed to deduce the following parameters: $H_{0hf} = 216$ kOe, $T_N = 248$ K, $b = 0.2$. The solid line in Fig. 7 represents the best fitting of the data obtained by the least-squares procedure. These data clearly show that the magnetic phase transition occurs at 248 K.

The hyperfine parameters of $RbFeSe_2$ conform well with Mössbauer results for the related alkali-metal and thallium-iron sulfides and selenides (see Table III) [17,28,36]. Note that the hyperfine-field value of 216 Oe is significantly smaller than that one, $H_{0hf}(S = 5/2) \sim 515$ kOe, for high-spin Fe^{3+} in ionic oxide compounds (see Ref. [57], chap. 7). At the same time, it is twice as large as the hyperfine field $H_{0hf}(S = 1/2) \sim 110$ kOe expected for the $S = 1/2$ low-spin state. Such a reduced value of the hyperfine field indicates a strong reduction of the local iron-spin moment in $RbFeSe_2$.

The temperature dependence of the spectral area associated with the $RbFeSe_2$ chains is shown in the inset of Fig. 7. It is smoothly varying over the entire temperature range, but there is some discontinuity at the transition temperature, $T_N = 248$ K. The temperature dependence of the Mössbauer spectral area follows the dependence of the Lamb-Mössbauer factor f_M versus temperature. In the standard Debye approximation,

TABLE III. Comparison of Mössbauer parameters for $AFeX_2$ (A = K, Rb, Cs, Tl; X = S, Se) [17,28,36]. Isomer shift IS and quadrupole splitting QS at room temperature (RT), hyperfine field H_{0hf} at $T = 4$ K. The ordered moment μ_{ord} is taken from Table I.

Sample	IS (mm/s) at RT	QS (mm/s) at RT	H_{0hf} (kOe) at 4 K	μ_{ord} (μ_B)
$KFeS_2$	0.21	0.51	215	2.43
$RbFeS_2$	0.20	0.45	196	1.83
$CsFeS_2$	0.21	0.44	193	1.88
$TlFeS_2$	0.05	0.53	163	1.85
$KFeSe_2$	0.34	0.44	218	3
$RbFeSe_2$	0.24	0.34	216	2.66

the recoilless fraction f_M can be expressed by (Ref. [57], chap. 4)

$$f_M = \exp\left\{-\frac{3E_R}{2k_B\Theta_D^M}\left[1+4\left(\frac{T}{\Theta_D^M}\right)^2\int_0^{\Theta_D^M/T}\frac{xdx}{(e^x-1)}\right]\right\}, \quad (2)$$

where k_B is Boltzmann constant, Θ_D^M is the Debye temperature, and E_R is the recoil energy of a free emitting nucleus.

The results of the least-squares fit by Eq. (2) are presented in the inset of Fig. 7 by solid lines for the temperature range below the transition temperature and above the transition point. The Debye temperature Θ_D^M for the region below $T_N = 248$ K is deduced from the experimental data by the least-squares fitting procedures as $\Theta_D^M = 223$ K, whereas for the temperature range above T_N it is $\Theta_D^M = 194$ K. The values of Θ_D^M found here are markedly larger than the Θ_D values derived from our specific-heat measurements. We may notice here that the Mössbauer effect (nuclear gamma-resonance) is affected only by the iron-nucleus motion being some kind of local probe of lattice vibrations. One can assume that the low-frequency acoustic-phonon density of states is quite low at the iron site, because the $FeSe_4$ tetrahedra are the most rigid units of the $RbFeSe_2$ lattice structure. Dominating high-frequency vibrations of the iron sites may come out through elevated Debye temperature Θ_D^M when described in the standard Debye approximation, Eq. (2). Magnetic ordering within the Fe subsystem brings additional rigidity into the chains of $FeSe_4$ tetrahedra increasing local vibration frequencies and, thus, further raising the Debye frequency Θ_D^M.

III. CONCLUSION

Our detailed preparative, structural, magnetic, specific-heat, and Mössbauer spectroscopy studies of $RbFeSe_2$ single crystals revealed important properties and peculiarities of this material. The results of the magnetic characterization of this linear-chain system may be summarized as follows:

(1) The magnetic susceptibility shows apparent quasi-1D properties in the paramagnetic regime and the occurrence of 3D magnetic order with the magnetic moments aligned perpendicularly to the chains below $T_N = 248$ K.

(2) The temperature dependence of the specific heat is well described in terms of one Debye and two Einstein oscillators. The increased weight of the Debye oscillator was ascribed to the contribution of AFM magnons. The only small anomaly and corresponding low value of entropy at T_N indicates a significant spin reduction and the existence of AFM fluctuations even far above T_N.

(3) The Mössbauer measurements access the magnetic and elastic properties microscopically at the Fe site. The small value of the hyperfine field corroborates the strong spin reduction of Fe^{3+}. The larger values of the Debye temperature determined from the spectral area as compared to the specific-heat data probably result from the rigidity of the $FeSe_4$ units.

We suggest that $RbFeSe_2$ is on the verge of being a quasi-one-dimensional metal. The main argument in favor of the metallic behavior is the temperature dependence of the magnetic susceptibility, which increases linearly from the Néel temperature up to the highest temperature ($T = 720$ K) accessible in our measurements and does not show any tendency for saturation. Comparing this behavior with quasi-1D organic conductors as well as with metallic quasi-2D iron pnictides and selenides, we expect the large intrachain Fe-Fe exchange interaction to promote 1D metallic conductivity which, however, is terminated by defects and breaks in the chains.

ACKNOWLEDGMENTS

The authors thank Dana Vieweg for SQUID and x-ray measurements and Yu. V. Lysogorskiy for discussion on the phonons in $RbFeSe_2$. This work was supported partly by the German Research Foundation (DFG) within the Transregional Collaborative Research Center TRR 80 "From Electronic Correlations to Functionality" (Augsburg-Munich-Stuttgart). Z.S. received financial support from German Academic Exchange Service (DAAD, Research Stays for University Academics and Scientists 2015). The work of F.G.V. and L.R.T. was supported by the Russian Government Program of Competitive Growth of Kazan Federal University. The work of A.G.K. was funded by the subsidy of the Ministry of Education and Science of the Russian Federation allocated to Kazan Federal University.

[1] Y. Kamihara, T. Watanabe, M. Hirano, and H. Hosono, J. Am. Chem. Soc. **130**, 3296 (2008).
[2] E. Dagotto, Rev. Mod. Phys. **85**, 849 (2013).
[3] G. Stewart, Rev. Mod. Phys. **83**, 1589 (2011).
[4] M. Fang, H. Wang, C. Dong, and Q. Huang, J. Phys.: Conf. Ser. **449**, 012015 (2013).
[5] H. Ryu, H. Lei, A. I. Frenkel, and C. Petrovic, Phys. Rev. B **85**, 224515 (2012).
[6] I. I. Mazin, D. J. Singh, M. D. Johannes, and M. H. Du, Phys. Rev. Lett. **101**, 057003 (2008).
[7] Y. J. Yan, M. Zhang, A. F. Wang, J. J. Ying, Z. Y. Li, W. Qin, X. G. Luo, J. Q. Li, J. Hu, and X. H. Chen, Sci. Rep. **2**, 212 (2012).
[8] J. Guo, S. Jin, G. Wang, S. Wang, K. Zhu, T. Zhou, M. He, and X. Chen, Phys. Rev. B **82**, 180520(R) (2010).
[9] M. Fang, H. Wang, C. Dong, Z. Li, C. Feng, J. Chen, and H. Yuan, Europhys. Lett. **94**, 27009 (2011).
[10] H. Takahashi, A. Sugimoto, Y. Nambu, T. Yamauchi, Y. Hirata, T. Kawakami, M. Avdeev, K. Matsubayashi, F. Du, C. Kawashima, H. Soeda, S. Nakano, Y. Uwatok, Y. Ueda, T. Sato, and K. Ohgushi, Nat. Mater. **14**, 1008 (2015).
[11] Mark R. Harrison and M. Grazia Francesconi, Coord. Chem. Rev. **255**, 451 (2011).
[12] Mark Robert Harrison, One-dimensional, mixed-metal sulphides—Structural and physical properties, Ph.D. thesis, The University of Hull, Kingston upon Hull, 2011.
[13] W. Bronger, J. Ruschewitz, and P. Müller, J. Alloys Compd. **218**, 22 (1995).

[14] K. Klepp and W. Bronger, Z. Anorg. Allg. Chem. **532**, 23 (1986).
[15] W. Bronger and P. Müller, J. Alloys Compd. **246**, 27 (1997).
[16] W. Klepp, W. Sparlinek, and P. Boller, J. Alloys Compd. **238**, 1 (1996).
[17] D. Welz, P. Deppe, W. Schaefer, H. Sabrowsky, and M. Rosenberg, J. Phys. Chem. Solids **50**, 297 (1989).
[18] W. Bronger, Pure Appl. Chem. **57**, 1363 (1985).
[19] I. R Shein and A. L. Ivanovskii, J. Supercond. Nov. Magn. **24**, 2215 (2011).
[20] D. Welz, S. Bennigton, and P. Müller, Physica B **213-214**, 339 (1995).
[21] H.-H. Schmidtke, U. Rossellen, and M. Diehl, Mol. Phys. **83**, 1191 (1994).
[22] W. Bronger, A. Kyus, and P. Müller, J. Solid State Chem. **70**, 262 (1987).
[23] W. Bronger, Angew. Chem. **20**, 52 (1981).
[24] S. K. Tiwary and S. Vasudevan, Phys. Rev. B **56**, 7812 (1997).
[25] Z. Seidov, H.-A. Krug von Nidda, J. Hemberger, A. Loidl, G. Sultanov, E. Kerimova, and A. Panfilov, Phys. Rev. B **65**, 014433 (2001).
[26] E. B. Asgerov, N. T. Dang, A. I. Beskrovnyy, A. I. Madadzada, D. I. Ismayilov, R. N. Mehdiyeva, S. H. Jabarov, and E. M. Karimova, Semiconductors **49**, 879 (2015).
[27] M. Nishi and Y. Ito, Solid State Commun. **30**, 571 (1979).
[28] M. Nishi, Y. Ito, and S. Fanahashi, J. Phys. Soc. Jpn. **52**, 2210 (1983).
[29] D. Welz, M. Kohgi, Y. Endoh, M. Nishi, and M. Arai, Phys. Rev. B **45**, 12319 (1992).
[30] D. Welz, S. Itoh, and A. D. Taylor, Europhys. Lett. **34**, 293 (1996).
[31] D. Welz and M. Nishi, Phys. Rev. B **45**, 9806 (1992).
[32] D. Welz, M. Winkelmann, H. M. Mayer, and M. Nishi, Physica B **234-236**, 576 (1997).
[33] J. Rodriguez-Carvajal, Physica B **192**, 55 (1993).
[34] L. Pauling, *The Nature of Chemical Bond* (Cornell University Press, Ithaca, NY, 1940).
[35] D. Klepp and H. Boller, Monatsh. Chem. **110**, 1045 (1979).
[36] H. Nissen and P. Nagorny, Z. Phys. Chem. Neue Folge **99**, 209 (1976).
[37] M. Dumm, A. Loidl, B. W. Fravel, K. P. Starkey, L. K. Montgomery, and M. Dressel, Phys. Rev. B **61**, 511 (2000).
[38] S. Nishioka, H. Kuriyaki, and K. Hirakawa, Synth. Met. **71**, 1877 (1995).
[39] S. Nishioka and K. Hirakawa, Jpn. J. Appl. Phys. **32**, L1150 (1993).
[40] K. Mimura, S. Motonami, Y. Shim, K. Wakiata, Z. Jahangirli, O. Alekperov, N. Mamedov, H. Sato, Y. Utsumi, S. Ueda, K. Shimida, Y. Taguchi, K. Kobayshi, G. Bihlmayer, H. Namatane, and M. Taniguchi, Phys. Status Solidi C **10**, 989 (2013).
[41] W. Malaeb, T. Yoshida, T. Kataokau, A. Fujimori, M. Kubota, K. Ono, H. Usui, K. Kuroki, R. Arita, H. Aoki, Y. Kamihara, M. Hirano, H. Usui, and H. Hosono, J. Phys. Soc. Jpn. **77**, 093714 (2008).
[42] S. de Jong, Y. Huang, R. Huisman, F. Massee, S. Thirupathaiah, M. Gorgoi, F. Schaefers, R. Follath, J. B. Goedkoop, and M. S. Golden, Phys. Rev. B **79**, 115125 (2009).
[43] X. F. Wang, T. Wu, G. Wu, H. Chen, Y. L. Xie, J. J. Ying, Y. J. Yan, R. H. Liu, and X. H. Chen, Phys. Rev. Lett. **102**, 117005 (2009).
[44] M. Rotter, M. Tegel, D. Johrendt, I. Schellenberg, W. Hermes, and R. Pöttgen, Phys. Rev. B **78**, 020503(R) (2008).
[45] R. Klingeler, N. Leps, I. Hellmann, A. Popa, U. Stockert, C. Hess, V. Kataev, H.-J. Grafe, F. Hammerath, G. Lang, S. Wurmehl, G. Behr, L. Harnagea, S. Singh, and B. Büchner, Phys. Rev. B **81**, 024506 (2010).
[46] G. M. Zang, Y. H. Su, Z. Y. Lu, Z. Y. Weng, D. H. Lee, and T. Xiang, Europhys. Lett. **86**, 37006 (2009).
[47] M. M. Korshunov, I. Eremin, D. V. Efremov, D. L. Maslov, and A. V. Chubukov, Phys. Rev. Lett. **102**, 236403 (2009).
[48] S.-P. Kou, T. Li, and Z.-Y. Weng, Europhys. Lett. **88**, 17010 (2009).
[49] S. L. Skornyakov, V. I. Anisimov, and D. Vollhardt, Phys. Rev. B **86**, 125124 (2012).
[50] V. Tsurkan, J. Deisenhofer, A. Günther, H.-A. Krug von Nidda, S. Widmann, and A. Loidl, Phys. Rev. B **84**, 144520 (2011).
[51] H.-D. Wang, C.-H. Dong, Z.-J. Li, Q.-H. Mao, S.-S. Zhu, C.-M. Feng, H.-G. Yuan, and M.-H. Fang, Europhys. Lett. **93**, 47004 (2011).
[52] J. M. Ziman, *Electrons and Phonons, the International Series of Monographs on Physics*, Vols. 9–11 (Clarendon Press, Oxford, 1960).
[53] D. C. Johnston, S. C. Mraw, and A. J. Jacobson, Solid State Commun. **44**, 255 (1982).
[54] M. Aldzhanov, N. Guseinov, G. Sultanov, and M. Nadzafzade, Phys. Status Solidi B **159**, K107 (1990).
[55] F. Du, K. Ohgushi, Y. Nambu, T. Kawakami, M. Avdeev, Y. Hirata,, Y. Watanabe, T. J. Sato, and Y. Ueda, Phys. Rev. B **85**, 214436 (2012).
[56] H. Lei, H. Ryu, A. I. Frenkel, and C. Petrovic, Phys. Rev. B **84**, 214511 (2011).
[57] G. K. Wertheim, *Mössbauer Effect: Principles and Applications* (Academic Press, New York, 1964).